1

2

3

4

5

6   **Age-related differences in myeloarchitecture measured at 7 T**

7

8   Andrew J. Carradus[1], Olivier Mougin[1], Benjamin A.E. Hunt[1], Prejaas K. Tewarie[1], Nicolas Geades[2],

9   Peter G. Morris[1], Matthew J. Brookes[1], Penny A. Gowland[1], & Christopher R. Madan[1,3]

10

11

12   [1] Sir Peter Mansfield Imaging Centre, School of Physics and Astronomy, University of

13   Nottingham, Nottingham, UK

14   [2] Philips Clinical Science, Philips Healthcare, Eindhoven, The Netherlands

15   [3] School of Psychology, University of Nottingham, Nottingham, UK

16

17

18

19   * Corresponding author.

20   Christopher R. Madan

21   School of Psychology, University Park

22   University of Nottingham

23   Nottingham, NG7 2RD, UK.

24   Email: christopher.madan@nottingham.ac.uk.

Abstract

We have used the magnetisation transfer (MT) MRI measure as a primary measure of myelination in both the grey matter (GM) of the 78 cortical automated anatomical labelling (AAL) regions of the brain, and the underlying white matter in each region, in a cohort of healthy adults (aged 19 to 62 years old). The results revealed a significant quadratic trend in myelination with age, with average global myelination peaking at 42.9 years old in grey matter, and at 41.7 years old in white matter. We also explored the possibility of using the Nuclear Overhauser Enhancement (NOE) effect, which is acquired in a similar method to MT, as an additional measure of myelination. We found that the MT and NOE signals were strongly correlated in the brain and that the NOE effects displayed similar (albeit weaker) parabolic trends with age. We also investigated differences in cortical thickness with age, and confirmed a previous result of a linear decline of 4.5±1.2μm/year.

42 **1   Introduction**

43   Many aspects of brain structure vary systematically as a function of age, such as cortical thickness,

44   gyrification, subcortical volume, and white matter tract integrity (Bartzokis et al., 2012; de Mooij et

45   al., 2018; Fjell et al., 2009; Hogstrom et al., 2013; Madan & Kensinger, 2016, 2017, 2018; Salat et al.,

46   2004; Tamnes et al., 2010). Foundational work in the early 1900s used post-mortem histological

47   techniques on small numbers of individuals to show age-related differences in cortical myelination

48   (Kaes, 1907), and also provided insights into related topology (Campbell, 1905; Flechsig, 1920; Hopf,

49   1955; Vogt, 1906). However the data remain sparse and in vivo measures are really required to enable

50   proper study across the life span.

51   Magnetic resonance imaging (MRI) provides a range of markers of myeloarchitecture and

52   myelination *in vivo* (Armstrong et al., 2004; Callaghan et al., 2014; Dick et al., 2012; Glasser & Van

53   Essen, 2011; Mangeat et al., 2015; Sanchez-Panchuelo et al., 2012) and thus provides a unique

54   opportunity to study differences in brain myelination through life (Callaghan et al., 2014; Draganski et

55   al., 2011; Grydeland et al., 2013). These studies used ratio of T_1 vs. T_2 intensity or magnetisation

56   transfer sequences to observe widespread age-related differences in myelination. Earlier work (Cho

57   et al., 1997) observed a quadratic trend with *in vivo* human brain T_1 measurements with age, however

58   they suggested that this differences could originate in other factors beyond myelination including

59   differences in membrane lipid content, brain volume, and cortical iron content. Another study

60   (Yeatman et al., 2014) measured T_1 in white matter fascicles and also found a parabolic trend with

61   age, while in addition showing that T_1 measurements were correlated to macromolecule tissue

62   content. Previous work (Bartzokis et al., 2012) showed differences in T_2 and diffusion measured during

63   the life span related to brain development and brain repair, but T_2 is strongly affected by iron content

64   and diffusion measures depend on axonal geometry.

65   Magnetisation transfer (MT) imaging has been used to study myelination in a number of prior

66   studies (Armstrong et al., 2004; Callaghan et al., 2014; Zaretskaya et al., 2018), providing an advantage

67   over T_1 based measures in that when quantified correctly, the quantitative MT signal is not affected

68   by cortical iron content (Lorio et al., 2014). Here we sought to examine age-related differences in

69   myelination at 7 T using both quantitative MT and the related Nuclear Overhauser Enhancement

70   (NOE) effect and provide more specific regional estimates of these effects.

71   While conventional MRI observes the properties of unrestricted cellular ('free') water protons,

72   there are other 'bound' protons that also contribute to the MR signal. These consist of both

73   macromolecular protons, and certain water protons which have their motion restricted through

74   hydrogen bonding to the macromolecular surface. We can probe the presence of these

75   macromolecules via the MT effect (Wolff & Balaban, 1989), by selectively saturating the bound

76   protons (which resonate at a frequency which is off-resonance from free water). As the bound protons

77   return to equilibrium they can transfer their magnetisation to free water, primarily through dipole-

78   dipole interactions (Edzes et al., 1977), and the resulting reduction in the free water signal can be

79   detected using conventional MRI methods.

80   The NOE signal is acquired in a similar way, except that the NOE signal corresponds to protons

81   resonating specifically at -3.5ppm with respect to water (Jones et al., 2013). Details of the physical

82   origins of this signal are given elsewhere, but in short the NOE signal occurs when energy is exchanged

83   between two spins that are very close together (~0.5nm), and it is generally associated with aliphatic

84   and olefinic protons (Desmond et al., 2014). NOE and MT signals seem to vary in a similar way in the

85   healthy brain, however this is not the case in all tissues (Shah et al., 2018). MRI at 7 T provides

86   increased sensitivity for MT and NOE effects and also higher signal-to-noise ratio (SNR) and hence

87   spatial resolution, which will improve sensitivity in studies of aging. Technical issues related to

88   increased specific absorption rate (SAR) and inhomogeneities in the B_1 transmit field can complicate

89   the measurements, and MT measurements can also be affected by variations in T_1 so the method of

90   quantification used here took account of B_1 and T_1 variations via a look up table.

91   In this study we aimed to investigate for the first time the variation of quantitative MT and

92   NOE signals over the mid-life age range and to compare it to differences in cortical thickness.

93

94   **2   Methods**

95   *2.1. Participants*

96   Ethical approval was granted by the University of Nottingham Medical School Research Ethics

97   Committee. From an initial recruitment of 77 people giving a written informed consent for a combined

98   MEG/MRI study (Hunt et al., 2016), 58 participants (aged 19 to 62 years old; 27 male; 52 right-handed)

99   successfully fulfilled complete data acquisition with satisfactory data quality on the FreeSurfer cortical

100 ribbon segmentation. Participants completed an online screening form to assess health and lifestyle,

101 which included the Edinburgh Handedness Inventory (Oldfield, 1971), and were excluded from the

102 study if they had current mental illness or diagnosis of mental illness within five years, any history of

103 neurological disorder, or family history of highly heritable mental illness (such as schizophrenia or

104 Huntington's Chorea). It was not feasible to exclude people with any history of mental illness due to

105 the high proportion of individuals who have, at some point, been diagnosed with a mental illness. This

106 study is based on additional analyses of MRI data from a previously published dataset comparing

107 magnetoencephalography and 7 T MRI (Hunt et al., 2016).

108 *2.2. MRI acquisition*

109   The MRI protocol has been described previously (Hunt et al., 2016), and is only summarised here.

110 Participants were scanned using a Philips Achieva 7 T system with the Phase Sensitive Inversion

111 Recovery sequence (PSIR: TI1/TI2=780ms/1600ms, 0.8mm isotropic voxels 240x216x160mm^3 field of

112 view) (Mougin et al., 2016) to delineate the cortex. MT and NOE were quantified by acquiring z-spectra

113 (Geades et al., 2016), which plot the water proton signal measured at progressively different off

114 resonance saturation frequencies. A z-spectrum was acquired using a magnetization transfer

115 prepared- turbo field echo (MT-TFE) sequence with a train of 20 off-resonance saturation pulses

116 (Gaussian-windowed sinc pulses, bandwidth 200Hz) applied at 17 frequency offsets in turn (0, ±1.0, -

117 2.3, +2.5, ±3, ±3.5, ±4.0, +4.5, -4.7, ±6.7 and ±16.7, and also +167 ppm acquired for normalization).

118 This was repeated at three nominal B_1 amplitudes ($B1_{rms}$= 0.38, 0.75, and 1.25 µT) to provide sensitivity

119 to effects more prevalent at high or low saturation powers (Geades et al., 2016). The TFE 3D imaging

120 readout (TE/TR/FA=2.7ms/5.8ms/8°) provided 1.5mm isotropic image resolution across a FOV of

121 $192 \times 192 \times 60 mm^3$. The total acquisition time was 24 minutes total for the three powers. The z-spectra

122 were motion corrected using FSL MCFLIRT (Woolrich et al., 2009) and B_0 corrected (Mougin et al.,

123 2010). They were then fitted to a database of spectra simulated using the Bloch-McConnell equations

124 (Geades et al., 2016). This fit resulted in a map of the estimate for the size of the bound proton pool

125 without contamination from chemical exchange saturation transfer (CEST) or NOE effects, and a

126 separate map of NOE effects.

127 *2.3. Image analysis*

128 The PSIR images were used to create a conservative grey matter (GM) mask and a white matter

129 (WM) mask with no overlap between them, using the boundary detection tool in FreeSurfer v5.3.0

130 (Dale et al., 1999; Fischl, 2012). If a voxel lay on the boundary between the grey and white matter, it

131 was excluded. PSIR images were then registered to the automated anatomical labelling (AAL) atlas

132 (Tzourio-Mazoyer et al., 2002) using FSL, and the mean cortical thickness was calculated for each

133 region within the AAL atlas, for each participant using FreeSurfer. Cortical thickness estimates were

134 averaged across the whole brain and plotted against participant age. This was repeated for each AAL

135 region separately and for data averaged across selections of AAL regions representative of each of the

136 four lobes in the brain. A linear fit of cortical thickness against age was performed for all these

137 conditions, and the *p*-values of the fit were calculated. False discovery rate (FDR) correction (α=.05)

138 was performed on the data from the individual AAL regions to correct for multiple comparisons. The

139 PSIR data was also used to provide an estimate T_1 by comparing the signal from both readouts to a

140 look-up table (Geades et al., 2016)

141 The MT maps were registered to the PSIR images and masked first with the conservative GM

142 or WM mask, and then with the cortical AAL atlas or its underlying subcortical regions, to produce 78

143 GM-only and 78 WM-only ROIs for each participant, and a mean MT value was calculated for each

144 region. MT was plotted against participant's age for both the whole GM, and averaged across regions

145 of interest (ROIs), corresponding to the four lobes as for cortical thickness. 14 regions of the brain

146 were excluded due to limited field of view or poor B_1 shimming in these areas (regions 1, 2, 24, 28, 32,

147 34, 35, 40, 63, 67, 71, 72, 73, 74 of the cortical AAL atlas primarily located at the base of the brain).

148 Data were fitted with linear and quadratic functions and p-values of the fits were estimated. An *F*-test

149 was performed to determine whether the quadratic fit described the data significantly better than the

150 linear fit, by comparing the R^2 of each fit considering the additional degree of freedom gained with a

151 quadratic model. The quadratic coefficient within any GM region where the quadratic fit was

152 significant was mapped onto a cortical surface. To explore spatial variability across the cortex in

153 individual participants, we also calculated the standard deviation of MT across grey and white matter

154 ROIs, and cortical thickness across the whole cortex and across the four lobes separately. This was

155 repeated for WM with the quadratic coefficient also projected onto the cortical surface to allow the

156 GM and WM differences to be compared. Finally, the participant-averaged MT in each GM region was

157 plotted against the participant-averaged MT in the WM for the corresponding AAL-based region. This

158 analysis was then repeated for the NOE data and the variation of T_1 with age was also investigated.

159 MT values for each GM-only and WM-only AAL ROI were averaged across all participants

160 (removing age as a variable), and this was repeated for NOE, cortical thickness and T_1. To investigate

161 the relationship between WM and GM, the GM values were plotted against the WM values for MT

162 and NOE separately, and a linear fit was performed. To investigate the relationship between MT and

163 NOE, MT values were linearly fitted against NOE values for all GM and WM regions together, and for

164 GM and WM regions separately. T_1 values were also plotted against MT values in every GM region. To

165 investigate whether cortex thickness was related to MT, a linear fit was performed to a plot of cortical

166 thickness against GM MT.

167 To explore variations across the cortex, the standard deviation in the values of MT was

168 calculated between the voxels within each ROI, and across the whole of the GM and WM was

169 calculated for each participant. These standard deviation values were plotted against age and a

170 quadratic fit was performed and compared to a linear regression with the F-test.

171

172   **3. Results**

173   *3.1 Age-related differences in cortical thickness, MT, NOE and T1*

174   Figure 1A and Table 1 shows that cortical thickness reduces with age at a rate of 4.5±1.2 μm

175   per year when averaged over the whole brain (p<.001), with significant linear trends displayed in all

176   lobes of the brain (p<.002) except the temporal lobes (p=.6), using an α=.05 cutoff for determining

177   significance.

178   Figure 1B-C shows age-related differences in MT. For grey matter, a quadratic model fitted

179   age-related trends better than a linear model for the whole brain and each of the four lobes (Table

180   2). The quadratic model also fitted better for most white matter, with the exception of the temporal

181   lobes (p=.055). The quadratic coefficients, p-values and the F-test results of each of these quadratic

182   fits across the different lobes are presented in Table 2. Figure 1A and B show that GM MT showed a

183   markedly different topological pattern of age-related differences in MT compared to cortical

184   thickness.

185   Figure 1B-C and Table 2 also shows that age-related trends for NOE were similar but

186   significantly weaker than for MT. As several of the regional models were non-significant, only the

187   global NOE trends are displayed. Figure S1A-B and Table 2 show that T_1 also varied quadratically with

188   age in GM and WM.

189   *3.2 Relationship between GM and WM within same AAL region*

190   Figure 2 shows that the MT in each AAL ROI, averaged across participants, varied linearly with MT

191   in the underlying WM for the same AAL region (R^2=.384, p<.0001). A similar relationship was observed

192   for NOE (R^2=.343, p<.0001).

193   *3.3 Relationship between NOE, cortical thickness, T1, and MT*

194   Figure S1C and D shows that in GM ROIs (averaged across participants) there was no correlation

195   between T_1 and MT (*p*>.9), but a negative linear correlation was observed for WM (*p*<.001, R^2=.23). If

196   only participants aged under 42 were considered for GM then a non significant linear trend was

197   observed (p=0.24)

198   Figure S2A shows that there is a strong linear relationship between MT and NOE averaging across

199   all participants for both GM and WM ROIs (R^2=.9478, p<.0001). This relationship was persisted when

200   considering either GM (R^2=.305, p<.0001) or WM (R^2=.282, p<.0001) ROIs alone.

201   No significant correlation was found between cortical thickness and GM MT averaging across all

202   participants for each ROI (R^2=.004 and p=.59 for a linear regression). However Figure S2B shows that

203   when this analysis was restricted to participants under the age of 42 years old, there was a trend for

204   cortical thickness to decrease as MT increased (R^2=0.056, p=0.055).

205   3.4 *Variation across the cortex*

206   Figure 3 and Table 1 and 3 shows the variation with age in standard deviation in cortical thickness

207   and MT values across the different regions. For cortical thickness (Figure 3A) only the occipital and

208   temporal lobes showed a significantly non-zero linear trend. Figure 3B shows that the standard

209   deviation of MT within the GM showed a significantly quadratic trend with age across the whole brain

210   and across all lobes except for the occipital lobes. Figure 3C shows that there was no difference in the

211   standard deviation of MT with age in WM (p>0.05; Table 3).

212

213   **4   Discussion**

214   It is well known that brain structural measures such as cortical thickness and gyrification vary

215   with age. Here we replicate previous reports of a decrease in cortical thickness with age (Fjell et al.,

216   2009; Hogstrom et al., 2013; Madan & Kensinger, 2016, 2018; Salat et al., 2004), and complement this

217   with two additional quantitative MRI measures related to tissue composition, magnetisation transfer

218   (MT) and Nuclear Overhauser Enhancement (NOE). MT is widely used to study demyelination in

219   Multiple Sclerosis patients (Levesque et al., 2010), and has been proven to be strongly correlated with

220   myelin content in the brain (Schmierer et al., 2007). Simple measures of MT such as MTR can also be

221   affected by the T_1 of the tissue but the quantitative MT measures used here are corrected for the

222   variations in water T_1 and hence are more specifically sensitive to myelination. This is important since

223   T_1 decreases as either myelin or iron content increase. It is known from histology and susceptibility

224   weighted MRI that iron deposition can continue until the age of 40 or even 60 years of age (Hallgren

225 & Sourander, 1958, Wang et al., 2012), and increases further in older age in some deep grey matter

226 areas (Hallgren & Sourander, 1958). In earlier life iron is required in myelin producton in

227 oligodendrocytes (Connor & Menzies, 1996), but later in life the iron accumulation may be more

228 pathological.

229   Our quantitative measures showed widespread differences in MT through midlife in the

230 cortical grey and white matter, and in contrast to the linear decrease in cortical thickness, these

231 followed a parabolic profile peaking at about 42 years of age (varying between 35-48 across different

232 brain regions). Where as MT values are expected to increase with myelination, T_1 is expected to

233 decrease with myelination (and with increasing iron). T_1 showed a minimum at 49 years in GM, and at

234 45 years in WM. The trends were similar across the whole brain but were stronger in the WM regions,

235 possibly because of the greater absolute MT value in those regions. These results suggest that

236 myelination increases until the age of about 40, which is consistent with evidence that the production

237 of oligodendrocytes can be associated with learning new skills (McKenzie et al., 2014). In later life

238 evidence from electron microscope preparations in non-human primates has related decreases in

239 myelination to the breakdowns in the myelin sheath and white-matter integrity (Peters, 2002; Peters

240 et al., 1996). This decrease in myelination appears to a key facet of the general cortical atrophy known

241 to occur with aging, as other mechanisms (e.g., a reduction of cortical neurons) have been ruled out

242 (Gefen et al., 2015; von Bartheld, 2018).

243   The age at which we observed peak MT agrees with the work of Yeatman et al. (Yeatman et

244 al., 2014), who found the maximum in $1/T_1$ in WM at ~40 years. Cho et al. (1997) also found a minimum

245 in T_1 at about 40 years in WM, but found a mimium at 60 years in cortex. We found that in general MT

246 and NOE peaked slightly later in GM than WM but the differences were small (Table 2). However

247 similar to Cho et al., we did observe T1 in GM to have a minimum at a later age (48.5 years). These

248 differences between MT and T1 will reflect the opposing effects of decreasing myelination (decreases

249 MT and increases T_1) and increasing iron (decreases T_1) in the brain in later life. The opposing effect

250 of myelination on MT and T_1 was seen in WM (Figure S1D) but not in GM (Figure S1C and E) again

251 probably reflecting the effect of varying iron concentration in GM with age and also across the cortex

252   (Cox & Gowland, 2010), as the data is plotted for each ROI averaged across all participants. These

253   results all suggest that quantitative MT is a more specific marker of myelination than T_1. It should be

254   noted that some MT measures (in particular the MT Ratio) can be dependent upon T_1, but the

255   quantitative method used here corrects for these effects (Geades et al., 2016). Furthermore, previous

256   studies (Tyler & Gowland, 2005) have shown that the macromolecular T1 has little effect on the

257   measured MT. The use of multiple MRI modalities (including qMT, T_1, susceptibility and T_2 mapping)

258   (Warntjes et al., 2016) would make it easier to tease appart the differences in iron and myelination

259   occuring in the brain with age. These findings build on previous work, such as Taubert et al. (2020),

260   where global changes in MT have been demonstrated in both grey and white matter in relation to age,

261   though this study examined mid- to old-age adults (ages 46-86) .

262   We found that the value of MT in each ROI (averaged across all participants) was correlated

263   with the MT measured in the underlying WM in the same ROI, and a similar result was found for NOE

264   (Figure 2). This is expected since the connectivity bewteen areas of GM is achieved primarilily by axons

265   in the underlying WM (for instance the u-fibres) and may suggest an additional means of studying

266   connectivity.

267   NOE is a relatively new measure, which has also been shown to vary with myelin concentration

268   in vivo, for example in the visual cortex (Mougin et al., 2013). The NOE signal in the brain is thought

269   to originate in transfer of magnetisation from aliphatic backbones of mobile macromolecules and

270   proteins, with the signal possibly relayed via molecular exchange (van Zijl et al., 2018). Here we found

271   that MT and NOE were well correlated across all GM and WM regions suggesting that similar

272   mechanisms were affecting them both. The fitting method used here models MT and NOE

273   simultaneously and thus minimises biasing of the NOE signal by MT. Furthermore this fitting method

274   has found this relationship between NOE and MT breaks down in blood where the NOE effect is

275   relatively larger (Shah et al., 2018). This suggests that NOE is correlated to myelination independent

276   of MT, and might relate to the fact that NOE is thought to be sensitive to the aliphatic groups in myelin.

277   The sensitivity of the NOE signal is lower than MT, but nonetheless, this measure has not yet been

278   explored fully and thus these results may play a role in planning future experiments.

279   The standard deviation in GM was an order of magnitude larger than that in white matter and

280   it seems likely that this reflects real variation across the ROI. The GM ROIs were smaller than the WM

281   ROIs which will have caused a larger standard error in both the mean and the standard deviation, but

282   will not influence the participant-averaged value of standard deviation. Furthermore the absolute

283   value of MT in GM was about half that in WM but we do not expect this to explain the increase the

284   absolute variance in the measurement and have shown that the interindividual variability is the same

285   in GM and WM MT measured with this method (Geades et al., 2016). There was a linear increase in

286   standard deviation in MT values across GM with age of about 30% (dominated by the period up to the

287   age 40), but no singificant difference in the standard deviation of MT in WM. We propose that this

288   increase in variation in MT with age reflects ongoing cortical plasticity over this period, for instance

289   relating to longitudinal changes in structural networks (Wu et al., 2013).

290   Although these results indicate that quantitative MT can be a more specific measure of

291   myelination, caution must be excercised when measuring MT. We acquired a full z-spectrum which is

292   a more specific measure than the conventional MT ratio (Geades et al., 2016), although the sampling

293   frequencies chosen were optimized to measure amide proton transfer as well as NOE and MT and so

294   more precise or quicker results could be achieved with further optimization of the sampling to study

295   myelination in future. It is likely that MT is also dependent on other macromolecules present in tissue,

296   for instance the MT signal will reduce with edema in pathology (Vavasour et al., 2011). A recent paper

297   showed that the MT ratio measure (MTR) did not correlate with myelin content in an experimental

298   model of demyelination (Fjær et al., 2015), although this experimental model used is likely to have

299   also caused T_1 differences that will also have affected the MTR measure. Nonetheless, the MT pool

300   size as measured here is not corrected for variations in the exchange rate of labile protons with free

301   water, which depend on temperature and pH (Ward & Balaban, 2000), but are not expected to vary

302   much in healthy individuals.

303   Finally, it is important to note that the cortical segmentation performed on a T_1-weighted

304   scan, such that a change in T_1 could potentially shift the pial surface (for instance an increase in cortical

305   iron with age, or myelination during development (Natu et al., 2019) could both reduce cortical

306   thickness). Since myelination varies across the cortical layer, such a shift of the boundary of the cortical

307   layer could bias the measurements of MT (Lorio et al., 2016), and indeed averaging across participants,

308   ROIs with higher MT tended to be thinner which may reflect differential myelination across the cortical

309   layer (Figure S2B). However to limit any effect of this, we used PSIR for segmentation which has

310   reduced sensitivity to proton density and T2* compared to the MPRAGE scan and the voxels at the

311   boundary of the cortical ribbon were excluded from the analysis. Future work could use a voxel based

312   analysis to study this grey/white boundary. However no correlation could be seen between the

313   coefficients of cortical thickness difference with age compared to MT differences with age when

314   considering solely thin, medium or thick cortical ribbon regions, suggesting that the cortical ribbon

315   thickness did not influence the MT results presented here.

316

317   **5. Conclusion**

318   We have used MT as a marker for myelination due to its reduced sensitivity to aspects of brain

319   structure other than myelin, and have shown that it has a strong parabolic trend with age in both GM

320   and WM, peaking on average at age 42. We also introduce the NOE effect as a possible marker for

321   myelination, however further work into the true origin of this signal is necessary to explore where this

322   measure may best be an asset.

323

324   **Acknowledgements**

328

329   **Disclosure Statement**: No conflicts of interest exist

330

References:

Armstrong, T. S., Cohen, M. Z., Weinberg, J., & Gilbert, M. R. (2004). Imaging techniques in neuro-oncology. *Seminars in Oncology Nursing*, *20*(4), 231–239.

Bartzokis, G., Lu, P. H., Heydari, P., Couvrette, A., Lee, G. J., Kalashyan, G., Freeman, F., Grinstead, J. W., Villablanca, P., Finn, J. P., Mintz, J., Alger, J. R., & Altshuler, L. L. (2012). Multimodal magnetic resonance imaging assessment of white matter aging trajectories over the lifespan of healthy individuals. *Biological Psychiatry*. https://doi.org/10.1016/j.biopsych.2012.07.010

Callaghan, M. F., Freund, P., Draganski, B., Anderson, E., Cappelletti, M., Chowdhury, R., Diedrichsen, J., FitzGerald, T. H. B., Smittenaar, P., Helms, G., Lutti, A., & Weiskopf, N. (2014). Widespread age-related differences in the human brain microstructure revealed by quantitative magnetic resonance imaging. *Neurobiology of Aging*. https://doi.org/10.1016/j.neurobiolaging.2014.02.008

CAMPBELL, H. (1905). PRINCIPLES OF HEREDITY: A REVIEW*. *British Journal of Inebriety*, *3*(1), 31–35. https://doi.org/doi:10.1111/j.1360-0443.1905.tb04399.x

Cho, S., Jones, D., Reddick, W. E., Ogg, R. J., & Grant Steen, R. (1997). Establishing norms for age-related changes in proton T1 of human brain tissue in vivo. *Magnetic Resonance Imaging*. https://doi.org/10.1016/S0730-725X(97)00202-6

Connor, J. R., & Menzies, S. L. (1996). Relationship of iron to oligodendrocytes and myelination. *GLIA*. https://doi.org/10.1002/(SICI)1098-1136(199606)17:2<83::AID-GLIA1>3.0.CO;2-7

Cox, E. F., & Gowland, P. A. (2010). Simultaneous quantification of T2 and T'2 using a combined gradient echo-spin echo sequence at ultrahigh field. *Magnetic Resonance in Medicine*. https://doi.org/10.1002/mrm.22522

Dale, A. M., Fischl, B., & Sereno, M. I. (1999). Cortical surface-based analysis: I. Segmentation and surface reconstruction. *NeuroImage*. https://doi.org/10.1006/nimg.1998.0395

de Mooij, S. M. M., Henson, R. N. A., Waldorp, L. J., & Kievit, R. A. (2018). Age differentiation within gray matter, white matter, and between memory and white matter in an adult life span cohort. *Journal of Neuroscience*. https://doi.org/10.1523/JNEUROSCI.1627-17.2018

Desmond, K. L., Moosvi, F., & Stanisz, G. J. (2014). Mapping of amide, amine, and aliphatic peaks in the CEST spectra of murine xenografts at 7 T. *Magnetic Resonance in Medicine*. https://doi.org/10.1002/mrm.24822

Dick, F., Tierney, A. T., Lutti, A., Josephs, O., Sereno, M. I., & Weiskopf, N. (2012). In vivo functional and myeloarchitectonic mapping of human primary auditory areas. *Journal of Neuroscience*. https://doi.org/10.1523/JNEUROSCI.1712-12.2012

Draganski, B., Ashburner, J., Hutton, C., Kherif, F., Frackowiak, R. S. J., Helms, G., & Weiskopf, N. (2011). Regional specificity of MRI contrast parameter changes in normal ageing revealed by voxel-based quantification (VBQ). *NeuroImage*. https://doi.org/10.1016/j.neuroimage.2011.01.052

Edzes, H. T., & Samulski, E. T. (1977). Cross relaxation and spin diffusion in the proton NMR of hydrated collagen [9]. In *Nature*. https://doi.org/10.1038/265521a0

Fischl, B. (2012). FreeSurfer. *NeuroImage*. https://doi.org/10.1016/j.neuroimage.2012.01.021

Fjær, S., Bø, L., Myhr, K. M., Torkildsen, O., & Wergeland, S. (2015). Magnetization transfer ratio does not correlate to myelin content in the brain in the MOG-EAE mouse model. *Neurochemistry International*. https://doi.org/10.1016/j.neuint.2015.02.006

Fjell, A. M., Walhovd, K. B., Fennema-Notestine, C., McEvoy, L. K., Hagler, D. J., Holland, D., Brewer, J. B., & Dale, A. M. (2009). One-year brain atrophy evident in healthy aging. *Journal of Neuroscience*. https://doi.org/10.1523/JNEUROSCI.3252-09.2009

377 Flechsig, P. E. (1920). *Anatomie des menschlichen Gehirns und Rückenmarks auf myelogenetischer*
378   *Grundlage* (Vol. 1). G. Thieme.

379 Geades, N., Hunt, B. A. E. E., Shah, S. M., Peters, A., Mougin, O. E., & Gowland, P. A. (2016).
380   Quantitative analysis of the z-spectrum using a numerically simulated look-up table:
381   Application to the healthy human brain at 7T. *Magnetic Resonance in Medicine*.
382   https://doi.org/10.1002/mrm.26459

383 Gefen, T., Gefen, T., Peterson, M., Papastefan, S. T., Martersteck, A., Whitney, K., Rademaker, A.,
384   Rademaker, A., Bigio, E. H., Bigio, E. H., Weintraub, S., Weintraub, S., Rogalski, E., Mesulam, M.
385   M., Mesulam, M. M., & Geula, C. (2015). Morphometric and Histologic Substrates of Cingulate
386   Integrity in Elders with Exceptional Memory Capacity. *Journal of Neuroscience*.
387   https://doi.org/10.1523/JNEUROSCI.2998-14.2015

388 Glasser, M. F., & Van Essen, D. C. (2011). Mapping human cortical areas in vivo based on myelin
389   content as revealed by T1- and T2-weighted MRI. *The Journal of Neuroscience : The Official*
390   *Journal of the Society for Neuroscience*. https://doi.org/10.1523/JNEUROSCI.2180-11.2011

391 Grydeland, H., Walhovd, K. B., Tamnes, C. K., Westlye, L. T., & Fjell, A. M. (2013). Intracortical myelin
392   links with performance variability across the human lifespan: Results from T1- and T2-
393   weighted MRI myelin mapping and diffusion tensor imaging. *Journal of Neuroscience*.
394   https://doi.org/10.1523/JNEUROSCI.2811-13.2013

395 Hallgren, B., & Sourander, P. (1958). THE EFFECT OF AGE ON THE NON-HAEMIN IRON IN THE HUMAN
396   BRAIN. *Journal of Neurochemistry*. https://doi.org/10.1111/j.1471-4159.1958.tb12607.x

397 Hogstrom, L. J., Westlye, L. T., Walhovd, K. B., & Fjell, A. M. (2013). The structure of the cerebral
398   cortex across adult life: Age-related patterns of surface area, thickness, and gyrification.
399   *Cerebral Cortex*. https://doi.org/10.1093/cercor/bhs231

400 Hopf, A. (1955). Über die Verteilung myeloarchitektonischer Merkmale in der isokortikalen
401   Schläfenlappenrinde beim Menschen. *J Hirnforsch*, *2*(1), 36–54.

402 Hunt, B. A. E., Tewarie, P. K., Mougin, O. E., Geades, N., Jones, D. K., Singh, K. D., Morris, P. G.,
403   Gowland, P. A., & Brookes, M. J. (2016). Relationships between cortical myeloarchitecture and
404   electrophysiological networks. *Proceedings of the National Academy of Sciences of the United*
405   *States of America*, *113*(47). https://doi.org/10.1073/pnas.1608587113

406 Jones, C. K., Huang, A., Xu, J., Edden, R. A. E., Schär, M., Hua, J., Oskolkov, N., Zacà, D., Zhou, J.,
407   McMahon, M. T., Pillai, J. J., & van Zijl, P. C. M. (2013). Nuclear Overhauser enhancement (NOE)
408   imaging in the human brain at 7T. *NeuroImage*.
409   https://doi.org/10.1016/j.neuroimage.2013.03.047

410 Kaes, T. (1907). *Die Grosshirnrinde des Menschen in ihren Maßen und ihrem Fasergehalt. Ein*
411   *gehirnanatomischer Atlas mit erläuterndem Text* [Book].

412 Levesque, I. R., Giacomini, P. S., Narayanan, S., Ribeiro, L. T., Sled, J. G., Arnold, D. L., & Pike, G. B.
413   (2010). Quantitative magnetization transfer and myelin water imaging of the evolution of acute
414   multiple sclerosis lesions. *Magnetic Resonance in Medicine*.
415   https://doi.org/10.1002/mrm.22244

416 Lorio, S., Lutti, A., Kherif, F., Ruef, A., Dukart, J., Chowdhury, R., Frackowiak, R. S., Ashburner, J.,
417   Helms, G., Weiskopf, N., & Draganski, B. (2014). Disentangling in vivo the effects of iron content
418   and atrophy on the ageing human brain. *NeuroImage*.
419   https://doi.org/10.1016/j.neuroimage.2014.09.044

420 Lorio, Sara, Kherif, F., Ruef, A., Melie-Garcia, L., Frackowiak, R., Ashburner, J., Helms, G., Lutti, A., &
421   Draganski, B. (2016). Neurobiological origin of spurious brain morphological changes: A
422   quantitative MRI study. *Human Brain Mapping*, *37*(5), 1801–1815.

423   https://doi.org/10.1002/hbm.23137

424 Madan, C. R., & Kensinger, E. A. (2016). Cortical complexity as a measure of age-related brain
425   atrophy. *NeuroImage*. https://doi.org/10.1016/j.neuroimage.2016.04.029

426 Madan, C. R., & Kensinger, E. A. (2017). Age-related differences in the structural complexity of
427   subcortical and ventricular structures. *Neurobiology of Aging*.
428   https://doi.org/10.1016/j.neurobiolaging.2016.10.023

429 Madan, C. R., & Kensinger, E. A. (2018). Predicting age from cortical structure across the lifespan.
430   *European Journal of Neuroscience*. https://doi.org/10.1111/ejn.13835

431 Mangeat, G., Govindarajan, S. T., Mainero, C., & Cohen-Adad, J. (2015). Multivariate combination of
432   magnetization transfer, T_2^* and B0 orientation to study the myelo-architecture of
433   the in vivo human cortex. *NeuroImage*. https://doi.org/10.1016/j.neuroimage.2015.06.033

434 McKenzie, I. A., Ohayon, D., Li, H., De Faria, J. P., Emery, B., Tohyama, K., & Richardson, W. D. (2014).
435   Motor skill learning requires active central myelination. *Science*.
436   https://doi.org/10.1126/science.1254960

437 Mougin, O., Abdel-Fahim, R., Dineen, R., Pitiot, A., Evangelou, N., & Gowland, P. (2016). Imaging gray
438   matter with concomitant null point imaging from the phase sensitive inversion recovery
439   sequence. *Magnetic Resonance in Medicine*, *76*(5). https://doi.org/10.1002/mrm.26061

440 Mougin, O. E., Coxon, R. C., Pitiot, A., & Gowland, P. A. (2010). Magnetization transfer phenomenon
441   in the human brain at 7 T. *NeuroImage*. https://doi.org/10.1016/j.neuroimage.2009.08.022

442 Mougin, Olivier, Clemence, M., Peters, A., Pitiot, A., & Gowland, P. (2013). High-resolution imaging of
443   magnetisation transfer and nuclear Overhauser effect in the human visual cortex at 7T. *NMR in
444   Biomedicine*. https://doi.org/10.1002/nbm.2984

445 Natu, V. S., Gomez, J., Barnett, M., Jeska, B., Kirilina, E., Jaeger, C., Zhen, Z., Cox, S., Weiner, K. S.,
446   Weiskopf, N., & Grill-Spector, K. (2019). Apparent thinning of human visual cortex during
447   childhood is associated with myelination. *Proceedings of the National Academy of Sciences*,
448   *116*(41), 20750–20759. https://doi.org/10.1073/PNAS.1904931116

449 Oldfield, R. C. (1971). The assessment and analysis of handedness: The Edinburgh inventory.
450   *Neuropsychologia*. https://doi.org/10.1016/0028-3932(71)90067-4

451 Salat, D. H., Buckner, R. L., Snyder, A. Z., Greve, D. N., Desikan, R. S. R., Busa, E., Morris, J. C., Dale, A.
452   M., & Fischl, B. (2004). Thinning of the cerebral cortex in aging. *Cerebral Cortex*.
453   https://doi.org/10.1093/cercor/bhh032

454 Sanchez-Panchuelo, R. M., Besle, J., Beckett, A., Bowtell, R., Schluppeck, D., & Francis, S. (2012).
455   Within-digit functional parcellation of brodmann areas of the human primary somatosensory
456   cortex using functional magnetic resonance imaging at 7 tesla. *Journal of Neuroscience*.
457   https://doi.org/10.1523/JNEUROSCI.2501-12.2012

458 Schmierer, K., Tozer, D. J., Scaravilli, F., Altmann, D. R., Barker, G. J., Tofts, P. S., & Miller, D. H.
459   (2007). Quantitative magnetization transfer imaging in postmortem multiple sclerosis brain.
460   *Journal of Magnetic Resonance Imaging*. https://doi.org/10.1002/jmri.20984

461 Shah, S. M., Mougin, O. E., Carradus, A. J., Geades, N., Dury, R., Morley, W., & Gowland, P. A. (2018).
462   The z-spectrum from human blood at 7T. *NeuroImage*, *167*.
463   https://doi.org/10.1016/j.neuroimage.2017.10.053

464 Taubert, M., Roggenhofer, E., Melie-Garcia, L., Muller, S., Lehmann, N., Preisig, M., Vollenweider, P.,
465   Marques-Vidal, P., Lutti, A., Kherif, F., & Draganski, B. (2020). Converging patterns of aging-
466   associated brain volume loss and tissue microstructure differences. Neurobiology of Aging, 88,
467   108–118. https://doi.org/10.1016/j.neurobiolaging.2020.01.006

468 Tamnes, C. K., Østby, Y., Fjell, A. M., Westlye, L. T., Due-Tønnessen, P., Walhovd, K. B., Ostby, Y., Fjell,

469   A. M., Westlye, L. T., Due-Tønnessen, P., & Walhovd, K. B. (2010). Brain maturation in
470   adolescence and young adulthood: regional age-related changes in cortical thickness and white
471   matter volume and microstructure. *Cerebral Cortex (New York, N.Y. : 1991)*.
472   https://doi.org/10.1093/cercor/bhp118

473   Tyler, D. J., & Gowland, P. A. (2005). Rapid quantitation of magnetization transfer using pulsed off-
474   resonance irradiation and echo planar imaging. *Magnetic Resonance in Medicine*.
475   https://doi.org/10.1002/mrm.20323

476   Tzourio-Mazoyer, N., Landeau, B., Papathanassiou, D., Crivello, F., Etard, O., Delcroix, N., Mazoyer,
477   B., & Joliot, M. (2002). Automated anatomical labeling of activations in SPM using a
478   macroscopic anatomical parcellation of the MNI MRI single-subject brain. *NeuroImage*.
479   https://doi.org/10.1006/nimg.2001.0978

480   van Zijl, P. C. M., Lam, W. W., Xu, J., Knutsson, L., & Stanisz, G. J. (2018). Magnetization Transfer
481   Contrast and Chemical Exchange Saturation Transfer MRI. Features and analysis of the field-
482   dependent saturation spectrum. *NeuroImage*.
483   https://doi.org/10.1016/j.neuroimage.2017.04.045

484   Vavasour, I. M., Laule, C., Li, D. K. B., Traboulsee, A. L., & MacKay, A. L. (2011). Is the magnetization
485   transfer ratio a marker for myelin in multiple sclerosis? *Journal of Magnetic Resonance
486   Imaging*. https://doi.org/10.1002/jmri.22441

487   Vogt, O. (1906). Über strukturelle Hirnzentra. *Mit Besonderer Berücksichtigung Der Strukturellen
488   Felder Des Cortex Pallii [On the Structural Centers of the Brain, with Particular Emphasis on the
489   Structural Regions of the Cortex]. Anatomischer Anzeiger*, *20*, 74–114.

490   von Bartheld, C. S. (2018). Myths and truths about the cellular composition of the human brain: A
491   review of influential concepts. In *Journal of Chemical Neuroanatomy*.
492   https://doi.org/10.1016/j.jchemneu.2017.08.004

493   Wang, D., Li, W. Bin, Wei, X. E., Li, Y. H., & Dai, Y. M. (2012). An Investigation of Age-Related Iron
494   Deposition Using Susceptibility Weighted Imaging. *PLoS ONE*.
495   https://doi.org/10.1371/journal.pone.0050706

496   Ward, K. M., & Balaban, R. S. (2000). Determination of pH using water protons and Chemical
497   Exchange Dependent Saturation Transfer (CEST). *Magnetic Resonance in Medicine*.
498   https://doi.org/10.1002/1522-2594(200011)44:5<799::AID-MRM18>3.0.CO;2-S

499   Warntjes, M., Engström, M., Tisell, A., & Lundberg, P. (2016). Modeling the presence of myelin and
500   edema in the brain based on multi-parametric quantitative MRI. *Frontiers in Neurology*.
501   https://doi.org/10.3389/fneur.2016.00016

502   Wolff, S. D., & Balaban, R. S. (1989). Magnetization transfer contrast (MTC) and tissue water proton
503   relaxation in vivo. *Magnetic Resonance in Medicine*. https://doi.org/10.1002/mrm.1910100113

504   Woolrich, M. W., Jbabdi, S., Patenaude, B., Chappell, M., Makni, S., Behrens, T., Beckmann, C.,
505   Jenkinson, M., & Smith, S. M. (2009). Bayesian analysis of neuroimaging data in FSL.
506   *NeuroImage*. https://doi.org/10.1016/j.neuroimage.2008.10.055

507   Wu, K., Taki, Y., Sato, K., Qi, H., Kawashima, R., & Fukuda, H. (2013). A longitudinal study of structural
508   brain network changes with normal aging. *Frontiers in Human Neuroscience*.
509   https://doi.org/10.3389/fnhum.2013.00113

510   Yeatman, J. D., Wandell, B. A., & Mezer, A. A. (2014). Lifespan maturation and degeneration of
511   human brain white matter. *Nature Communications*. https://doi.org/10.1038/ncomms5932

512   Zaretskaya, N., Fischl, B., Reuter, M., Renvall, V., & Polimeni, J. R. (2018). Advantages of cortical
513   surface reconstruction using submillimeter 7 T MEMPRAGE. *NeuroImage*.
514   https://doi.org/10.1016/j.neuroimage.2017.09.060

515

|		Linear coefficient (µm/year) ± 95% confidence intervals	p-value of linear trend
Cortical thickness	Global	-4.6 ± 1.2	.0004 *
	Frontal	-4.3 ± 1.4	.0028 *
	Parietal	-5.6 ± 1.7	.0019 *
	Occipital	-5.2 ± 1.3	.0002 *
	Temporal	1.0 ± 1.8	.59
Standard deviation in cortical thickness across the ROI	Global	-0.09 ± 0.01	.47
	Frontal	-0.3 ± 0.1	.058
	Parietal	-0.1 ± 0.2	.62
	Occipital	+0.49 ± 0.19	.015*
	Temporal	-0.47± 0.18	.011*

516
517 Table 1: Coefficients and significance of linear differences in cortical thickness with age globally across
518 the brain and in each lobe of the brain separately (* indicates a significant trend p<0.05)

|			Quadratic coefficient (x10-4 [MT%/NOE%/T1]2 / year) ± 95% confidence intervals	Age of peak (years)	p-value of quadratic trend vs. null hypothesis	p-value from F-test on quadratic model compared to linear model
MT	Grey matter	Global	-14 ± 3	42.9	.00002 *	.000005 *
		Frontal	-16 ± 4	41.9	.0008 *	.0005 *
		Parietal	-14 ± 4	40.6	.0009 *	.0007 *
		Occipital	-11 ± 4	45.8	.0074 *	.0023 *
		Temporal	-17 ± 7	45.2	.0115 *	.0044 *
	White matter	Global	-23 ± 5	41.7	.0001 *	.000001 *
		Frontal	-26 ± 8	41.3	.0011 *	.0008 *
		Parietal	-20 ± 6	41.1	.0025 *	.0019 *
		Occipital	-24 ± 7	43.8	.0005 *	.0002 *
		Temporal	-15 ± 9	44.6	.0847	.0546
NOE	Grey matter	Global	-5 ± 4	44.4	.016 *	.0078 *
		Frontal	-6 ± 8	47.0	.125	.0711
		Parietal	-6 ± 4	40.6	.003 *	.0022 *
		Occipital	-3 ± 82	45.4	.189	.1352
		Temporal	-5 ± 36	44.0	.092	.0641
	White matter	Global	-8 ± 5	40.9	.005 *	.0041 *
		Frontal	-13 ± 9	41.6	.005 *	.0033 *
		Parietal	-6 ±7	42.8	.066	.0495 *
		Occipital	-5 ±7	42.8	.1656	.1371
		Temporal	-4 ±.8	37.5	.341	.3704
T1	Grey matter	Global	1.7 ± 1.4	48.5	.005 *	.0006 *
	White matter	Global	0.74 ± 0.38	44.8	.00002 *	.000004 *

519 Table 2: Coefficients and significance of the quadratic model applied to differences in measured
520 MT, NOE and T_1 with age globally across the brain and in each lobe of the brain separately (*
521 indicates a significant non-zero trend $p<0.05$)

			Quadratic coefficient (x 10^{-4} MT%^{2} / year) ± 95% confidence intervals	Age of Peak (years)	p-value of quadratic trend vs. null hypothesis	p-value from F-test on quadratic model compared to linear model
MT	Grey Matter	Global	-5 ± 1	48.90	.000002 *	.000005 *
		Frontal	-5 ± 2	50.31	.00009 *	.0050 *
		Parietal	-5 ± 2	49.07	.00020 *	.0038 *
		Occipital	-2 ± 2	62.67	.00004 *	.1756
		Temporal	-9 ± 3	46.20	.00048 *	.0006 *
	White matter	Global	-0.1 ± 0.4	62.35	.1588	.7530
		Frontal	-0.4 ± 0.2	35.54	.1527	.0633
		Parietal	-0.3 ± 0.5	30.29	.4868	.6094
		Occipital	-0.2 ± 0.4	42.14	.8008	.6879
		Temporal	-0.9 ± 0.5	40.83	.1183	.0196 *

Table 3: Coefficients and significance of the quadratic model applied to differences in the standard deviation of measured MT with age globally across the brain and in each lobe of the brain separately (* indicates a significant non-zero trend p<0.05)
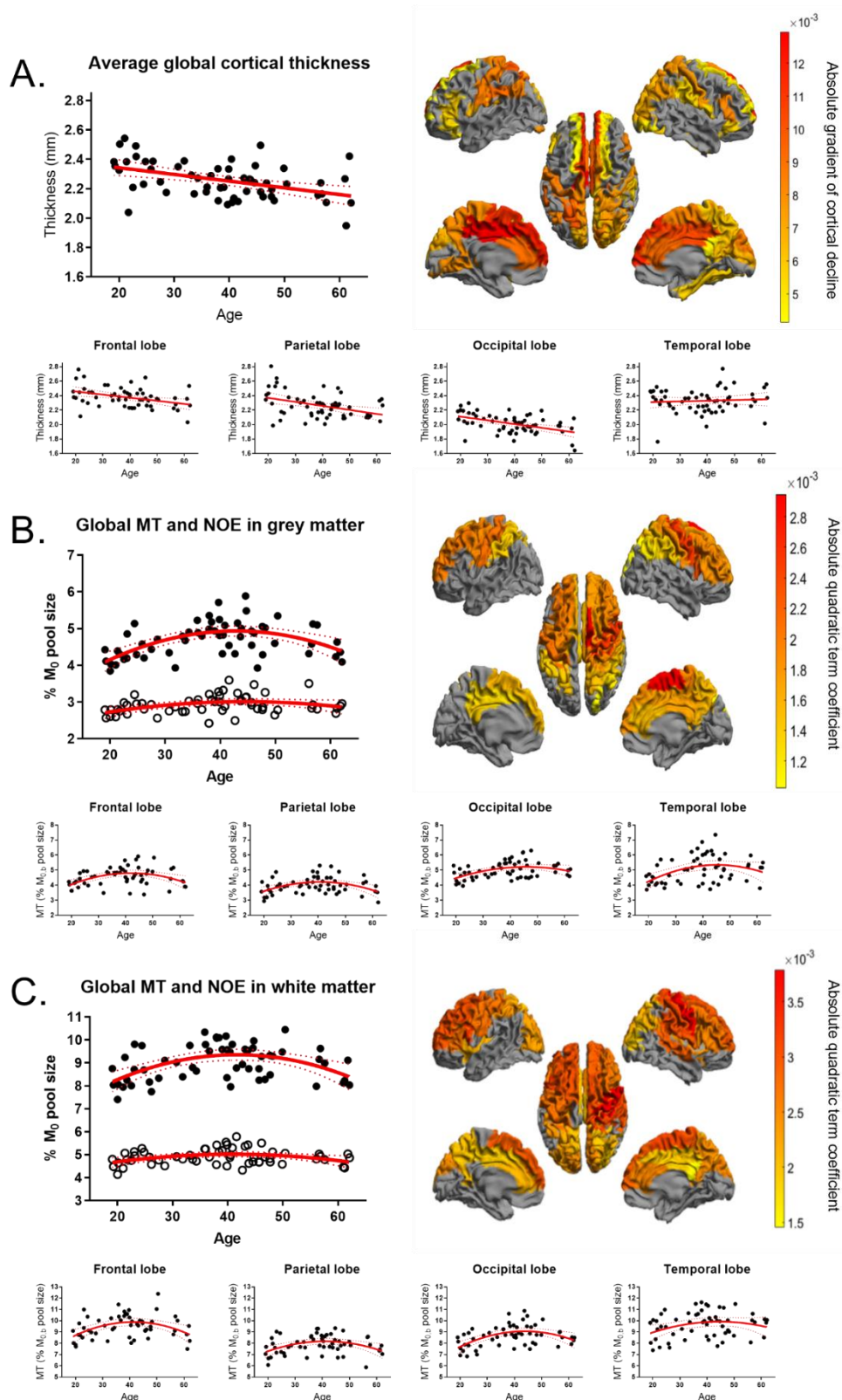
Figure 1. Age-related differences in (A) global and lobe-wise cortical thickness, and MT (closed circles) from (B) grey matter (C) and white matter. NOE values are also shown on the global curves (open circles). Dotted lines correspond to 95% confidence intervals. Also shown is the topology of age-related differences in MT (with the white matter map projected onto overlying grey matter); regions shown in grey did not exhibit a significant quadratic or linear trend.
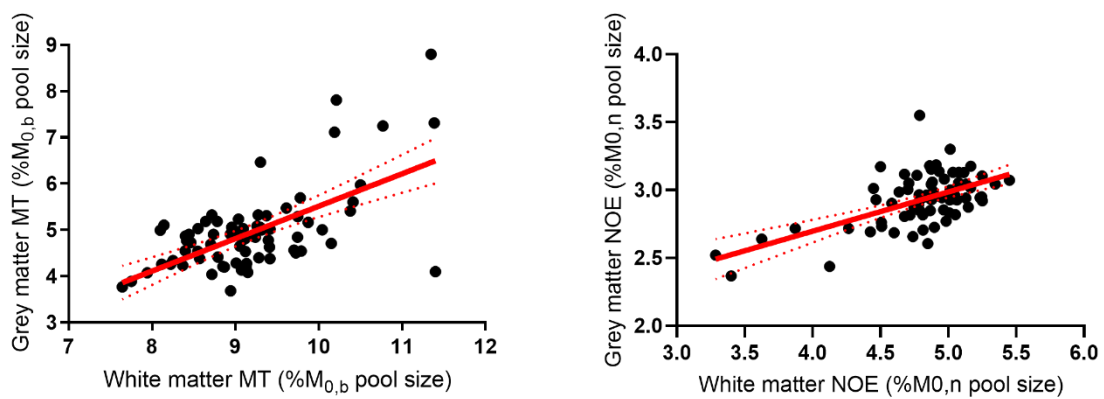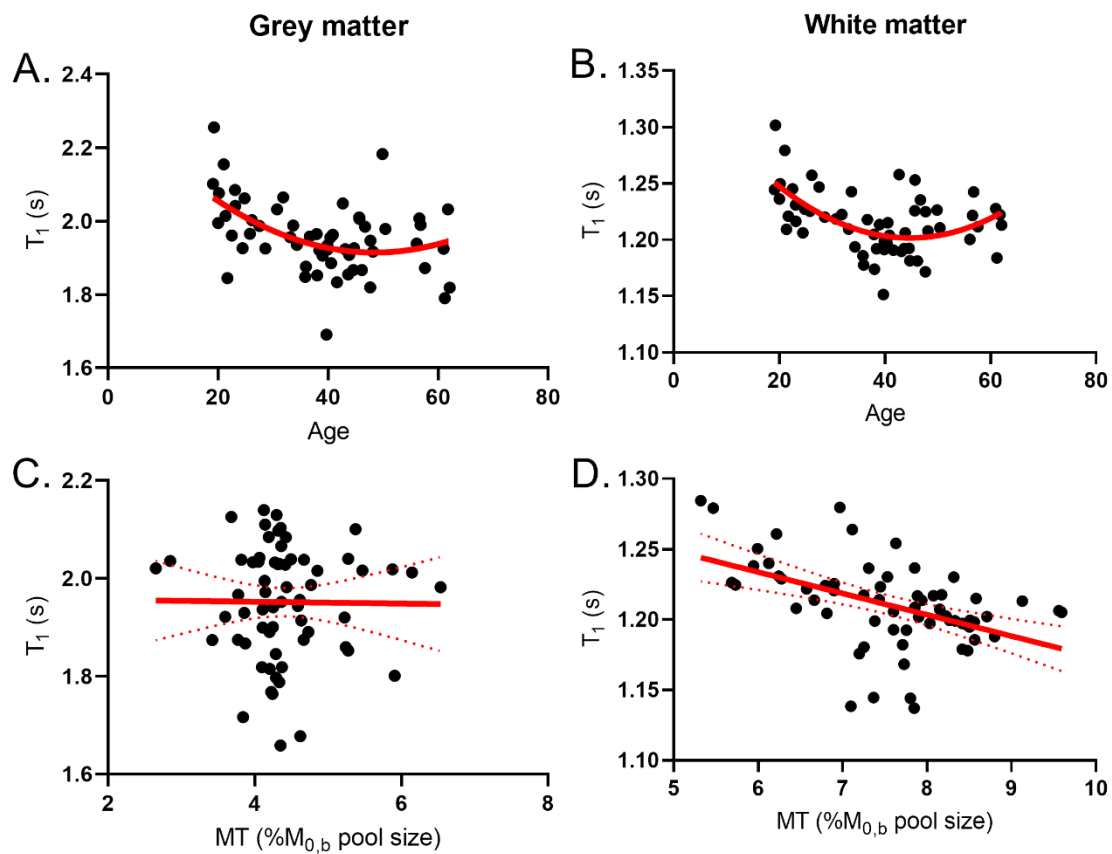
**Figure 2. Variation in MT (left) and NOE (right) in GM with that in underlying WM within the same AAL region, averaged across individuals for each AAL region.**
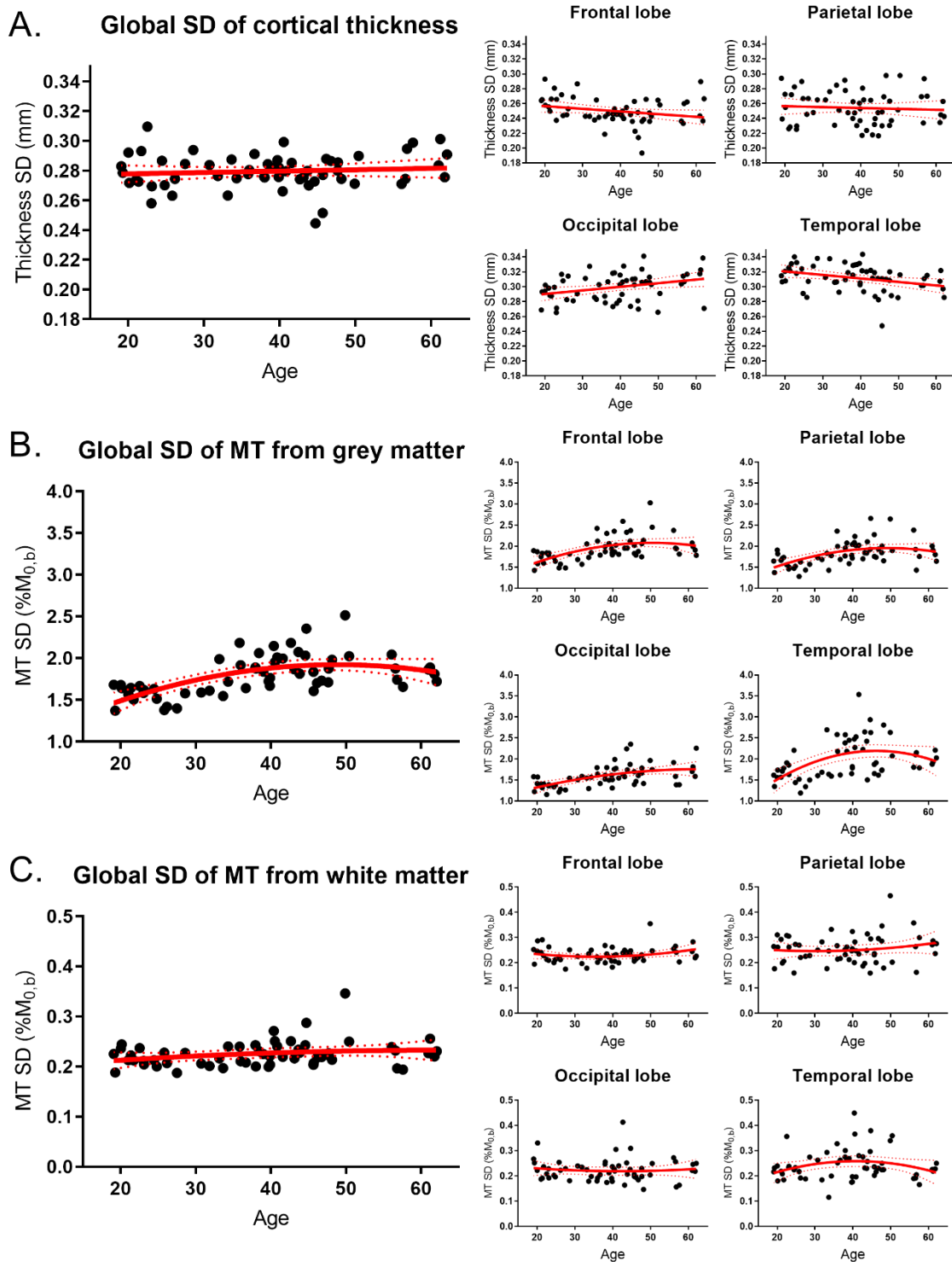
534
535 **Figure 3. Age-related variations in SD of global and lobe-wise (A) cortical thickness and MT from (B)**
536 **grey matter and (C) white matter.**

Figure S1. Age-related variations in T_1 of (A) global grey matter (B) and white matter, plotted for each participant separately. Variation of T1 with MT (plotted for each ROI averaged across participants) for (C) grey matter and (D) white matter.
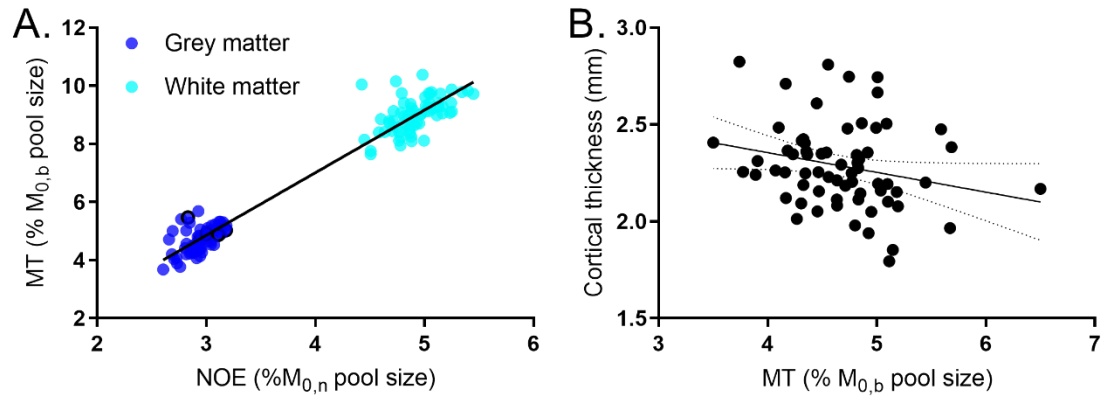
Figure S2. Correlation of MT vs. NOE for each AAL region averaged across individuals, shown in panel A. Panel B shows the variation in cortical thickness with GM MT for each AAL region, averaging across individuals aged under 42 years old only.